Lin, Bowen; Zheng, Mao; Han, Bing; Chu, Xiumin; Zhang, MY; Zhou, Haiming; Ding, Shigan; Wu, Hao; Zhang, Kehao

PSO-Based Predictive PID-Backstepping Controller Design for the Course-Keeping of Ships

PSO-Based Predictive PID-Backstepping Controller Design for the Course-Keeping of Ships

Bowen Lin [1,2], Mao Zheng [1,2,*], Bing Han [3], Xiumin Chu [1,2], Mingyang Zhang [4], Haiming Zhou [1,2], Shigan Ding [1,2], Hao Wu [1,2] and Kehao Zhang [1,2]

1   Intelligent Transportation Systems Research Center, Wuhan University of Technology, Wuhan 430062, China; linbw163@163.com (B.L.); zhouhaiming@whut.edu.cn (H.Z.)
2   National Engineering Research Center for Water Transport Safety, Wuhan 430070, China
3   National Engineering Research Center of Ship & Shipping Control System, Shanghai 200135, China
4   School of Engineering, Aalto University, 02150 Espoo, Finland
*   Correspondence: zhengmao@whut.edu.cn

Abstract: Ship course-keeping control is of great significance to both navigation efficiency and safety. Nevertheless, the complex navigational conditions, unknown time-varying environmental disturbances, and complex dynamic characteristics of ships pose great difficulties for ship course-keeping. Thus, a PSO-based predictive PID-backstepping (P-PB) controller is proposed in this paper to realize the efficient and rapid course-keeping of ships. The proposed controller takes the ship's target course, current course, yawing speed, as well as predictive motion parameters into consideration. In the design of the proposed controller, the PID controller is improved by introducing predictive control. Then, the improved controller is combined with a backstepping controller to balance the efficiency and stability of the control. Subsequently, the parameters in the proposed course-keeping controller are optimized by utilizing Particle Swarm Optimization (PSO), which can adaptively adjust the value of parameters in various scenarios, and thus further increase its efficiency. Finally, the improved controller is validated by carrying out simulation tests in various scenarios. The results show that it improves the course-keeping error and time-response specification by 4.19% and 9.71% on average, respectively, which can efficiently achieve the course-keeping of ships under various scenarios.

Keywords: ship course-keeping; MMG; PID control; predictive control; backstepping control; particle swarm optimization

1. Introduction

Maritime transportation holds a pivotal share of international trade [1,2]. As the most economical and effective tool of marine transport, it is essential that shipping increases constantly with the development of the national economy and international trade [3–5]. However, complex navigational conditions and unknown time-varying environmental disturbances pose a significant difficulty in the operation of ships [6–8]. Meanwhile, the complex dynamic characteristics (e.g., multiple degrees-of-freedom (DOF), nonlinearity, limitation in rudder angle) further increase the uncertainty of the ship's motion [9–14]. As a result, it is difficult to lead ships moving along a target course efficiently and accurately, especially under harsh environmental conditions [9,15–17]. Thus, it becomes indispensable to carry out research related to ship course-keeping.

To date, research on the course-keeping of ships mainly focuses on (a) improved traditional controllers and (b) data-driven controllers.

Improved traditional controllers are considered an effective approach to realize the course-keeping of ships. Some common methods include improved sliding mode controllers [18–21], improved PID controllers [20,22–24], improved backstepping controllers [9,25–27], and improved bipolar sigmoid functions [28,29]. These methods mainly improve traditional controllers by introducing adaptive control, synergetic control,

control formula improvement, and parameter optimization. However, these methods contain limitations such as a lack of course-keeping accuracy under environmental disturbances and inefficiency in reaching the target course, which may lead to additional course-keeping errors in some scenarios. At the same time, some controllers are complex to build and therefore less available.

Data-driven controllers become feasible for ship course-keeping control with the development of data acquisition and processing technologies. Methods adopted are known as expert knowledge controllers [30], artificial neural networks [31–35], neuro-fuzzy systems [36], and multi-agent systems [37]. These controllers are established based on empirical knowledge or navigation data. Researchers fused ship motion and operation data and processed it using various statistical and intelligent modeling methods to establish automatic ship course-keeping controllers. To improve the accuracy of course-keeping, these controllers have high requirements for the amount and quality of data in particular scenarios. As a result, such controllers are more effective in scenarios with a large amount of data on similar ships. Conversely, it is hard to realize accurate ship course-keeping in scenarios with less navigation data. Meanwhile, the selection of empirical knowledge or navigation data has a substantial impact on the effectiveness of ship course-keeping control, which further increases the uncertainty of the controller.

The above-mentioned controllers for the course-keeping of ships have been applied and validated. Nevertheless, difficulties such as obtaining the data required to train, and the high complexity to establish, limit the accuracy of the course-keeping controllers mentioned above. Additionally, some of the studies lack accuracy in establishing ship motion and environmental disturbance models for simulation tests, which prevents the effectiveness of those course-keeping controllers from being effectively verified [24,27].

Given these research gaps, in this paper, a PSO-based predictive PID-backstepping (P-PB) controller is introduced for the course-keeping of ships. The P-PB controller is designed on the basis of PID and backstepping controllers, thus retaining the simplicity and interpretability of traditional controllers. At the same time, course-overshoot of the controller is avoided by introducing a predictive PID control, which improves the accuracy of course-keeping. Subsequently, the parameters in the P-PB controller are optimized via PSO, which is characterized by its efficiency, and is widely used in the field of ship control to improve its applicability in various scenarios [38–40].

In Section 2, a nonlinear ship model is first introduced, which is adapted for ship motion prediction and simulation tests. Then, the improved PID controller and the backstepping controller are combined to design the P-PB controller. Further, PSO is introduced to optimize parameters in the proposed controller. Section 3 provides comparison tests with other controllers, demonstrating the effectiveness of our approach in various scenarios by using a case ship called KVLCC2. Section 4 serves as the conclusion, which engages in a discussion concerning the distinctive features and advantages of our proposed method, as applied to the field of ship course-keeping.

2. Methodology

The framework of the proposed P-PB controller for ship course-keeping (Figure 1) comprises three steps:

Step (i): Nonlinear ship model. A nonlinear ship model is established based on the MMG model. Consequently, an environmental disturbance model is introduced to simulate ship motion under time-varying disturbance conditions.

Step (ii): Course-keeping controller design. First, the PID control is improved based on a predictive control method. Then, the ship course-keeping controller is established by combining the improved PID and backstepping controllers, thus combining the advantages of both.

Step (iii): Parameter optimization of the ship course-keeping controller. The parameters in the proposed controller are adopted as input, and the minimization of the cumulative

course-keeping error is used as a fitness index. Then, the optimal control parameters for course-keeping in a particular scenario are obtained based on PSO.
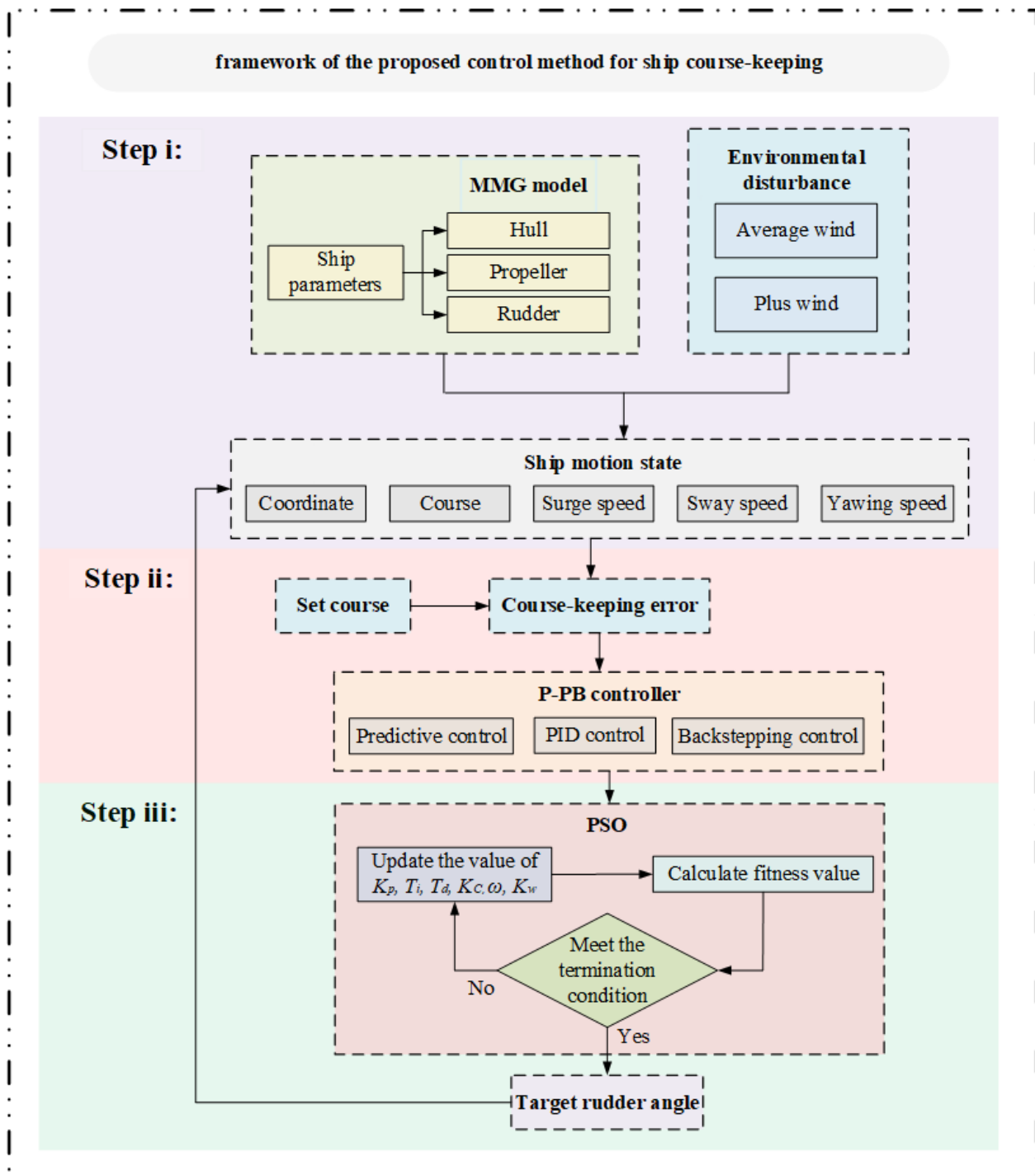
Figure 1. The framework of the proposed P-PB control method for ship course-keeping.

2.1. Nonlinear Ship Model

To simulate ship motion accurately, the ship motion model is established based on the MMG model. Then, the environmental disturbance model is introduced to simulate ship motion under various scenarios. A ship is typically considered a rigid body with six degrees of freedom (DOF) in motion. However, a three-degrees of freedom (3-DOF) ship dynamic model can be used when it comes to the control of ship motion along the

horizontal plane [41–43]. The course-keeping controller mainly changes the ship's motion along the horizontal plane; therefore, this paper is based on a 3-DOF nonlinear ship model.

The establishment of a nonlinear ship model contains three steps: the establishment of a ship motion coordinate system, kinematic modeling, and environmental disturbance modeling.

2.1.1. Ship Motion Coordinate System

The space-fixed coordinate system $O_0 - x_0 y_0$ and the ship-fixed coordinate system $O - xy$ are established, respectively, where the x_0 axis points directly north and the y_0 axis points directly east. In terms of the ship-fixed system, the x and y axes point towards the ship's bow and starboard, respectively.

u, v, and r are the ship's surge speed, sway speed, and yawing speed, respectively. ψ is the ship's course, which is defined as the angle between the x_0 and x axes. ψ_T is the wind direction. Finally, the ship-motion coordinate system is set up as in Figure 2.
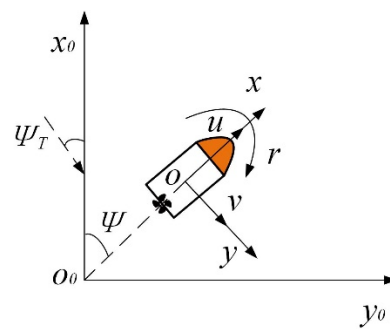

Figure 2. Coordinate system of ship motion.

2.1.2. Kinematic Model

The MMG model divides a ship into hull, propeller, and rudder. In addition, the effect of environmental disturbances on the ship's motion is also considered. Thus, the motion of a ship can be expressed as Equation (1):

$$
\begin{cases}
dx_t/dt = u\cos(\psi) - v\sin(\psi) \\
dy_t/dt = u\sin(\psi) + v\cos(\psi) \\
d\psi/dt = r \\
(m + m_x)\dot{u} - (m + m_y)vr = X_H + X_P + X_R + X_{wind} \\
(m + m_y)\dot{v} + (m + m_x)ur = Y_H + Y_P + Y_R + Y_{wind} \\
(I_{ZZ} + J_{ZZ})\dot{r} = N_H + N_P + N_R + N_{wind}
\end{cases}
\tag{1}
$$

where x_t and y_t are the position coordinates of origin in time t in the earth-fixed coordinate system. m is ship's mass. m_x and m_y are the added masses of the x and y axis directions. I_{ZZ} is the inertia moment of the ship, J_{ZZ} is the added moment of inertia. X_H, Y_H, and N_H are the surge force, sway force, and yaw moment acting on the ship's hull, respectively. X_P, Y_P, and N_P are the surge force, sway force, and yaw moment generated by the propeller. X_R, Y_R, and N_R are the surge force, sway force, and yaw moment generated by the rudder. X_{wind}, Y_{wind}, and N_{wind} are the wind load in the surge, sway, and yaw direction.

The calculation method of hull fluid force is shown in Equation (2).

$$
\begin{cases}
X_H = X(u) + X_{vv}v^2 + X_{vr}vr + X_{rr}r^2 \\
Y_H = Y_v v + Y_r r + Y_{|v|v}|v|v + Y_{|v|r}|v|r + Y_{|r|r}|r|r \\
N_H = N_v v + N_r r + N_{|v|v}|v|v + N_{vvr}v^2 r + N_{vrr}vr^2
\end{cases}
\tag{2}
$$

$X(u)$, X_{vv}, X_{vr}, X_{rr}, Y_v, Y_r, $Y_{|v|v}$, $Y_{|v|r}$, $Y_{|r|r}$, N_v, N_r, $N_{|v|v}$, N_{vvr}, and N_{vrr} are the hydrodynamic factors, which are determined by the empirical formulas proposed by Kijima [44].

By combining the methods proposed by Jia, Yang, and Brogliacan [45,46], the propeller force is calculated using Equation (3):

$$\begin{cases} X_P = \rho n_p^2 D_P^4 (1 - t_P) K_T(J_P) \\ Y_P = \rho n_p^2 D_P^4 K_T \sin(\arccos(u/v))/3 \\ N_P = 0.083 Y_P \end{cases} \tag{3}$$

where ρ is the density of water, t_P is the thrust deduction factor, D_P is the propeller diameter, J_P is the propeller advanced ratio, n_p is the propeller revolution, and K_T is the thrust coefficient of the propeller.

Subsequently, the rudder force is determined using Equation (4) [45]:

$$\begin{cases} X_R = (1 - t_R) F_N \sin \delta \\ Y_R = (1 + \alpha_H) F_N \cos \delta \\ N_R = (x_R + \alpha_H x_H) F_N \cos \delta \end{cases} \tag{4}$$

where t_R is the steering resistance deduction factor, α_H is the rudder force increase factor, x_R is the longitudinal coordinate of rudder position, x_H is the longitudinal coordinate of the acting point of the additional lateral force, F_N is the rudder normal force, and δ is the current rudder angle.

Additionally, due to the large resistance to movement, the turning speed of the rudder is limited [47]. Thus, the ship's rudder movement is characterized in Equation (5).

$$T_E \dot{\delta} = \delta_E - \delta \tag{5}$$

where T_E is the time constant, $\dot{\delta}$ is the rudder turning speed, and δ_E is the command rudder angle.

2.1.3. Environmental Disturbance Model

The operational performance of a ship is significantly vulnerable to external disturbances induced by wind, waves, and currents. However, a disturbance by currents mainly changes a ship's surge and sway speed and has less effect on its yawing moment, thus it can be ignored when it comes to control of a ship's course. In terms of waves, their height and frequency are closely related to the interference of wind. Therefore, the performance of a ship's course-keeping controller under wind disturbance represents a control effect under waves, to a certain extent. Moreover, it is difficult to accurately simulate the effect of wave disturbance on a ship's motion [48]. Consequently, the environmental disturbance model is established based on wind disturbance.

Wind disturbance can be divided into average wind and pulse wind. Between them, average wind is calculated according to the empirical formula in Equation (6) [49],

$$\begin{cases} \alpha_R = -\arctan(\frac{-v - V_R \sin(\psi_T - \psi)}{-u - V_R \cos(\psi_T - \psi)}) - v \\ F_{Xwind} = 0.5 C_x(\alpha_R) \rho_a V_R^2 A_F \\ F_{Ywind} = 0.5 C_y(\alpha_R) \rho_a V_R^2 A_L \\ N_{wind} = 0.5 C_m(\alpha_R) \rho_a V_R^2 A_L L \end{cases} \tag{6}$$

where α_R is the angle between the ship's course and the wind direction; v is the compensation angle of wind; $C_x(\alpha_R)$, $C_y(\alpha_R)$, $C_m(\alpha_R)$ is the wind load factor in surge, sway, and yaw direction; ρ_a is the density of air; V_R is the wind speed; A_F, A_L is the area of the ship exposed to wind in surge and sway direction; and L is the length of ship.

Then, white noise is introduced to calculate the pulse wind, which is calculated in Equation (7) [50]:

$$H(s) = 0.4198s/(s^2 + 0.3638s + 0.3675) \tag{7}$$

where s is the Laplace operator.

2.2. P-PB Course-Keeping Controller Design

The PID controller and the backstepping controller have their own advantages in various scenarios. In this paper, both the PID controller and the backstepping controller are taken into account when building the P-PB controller; thus, the advantages of the two controllers can be combined. The framework for the course-keeping controller is shown in Figure 3.
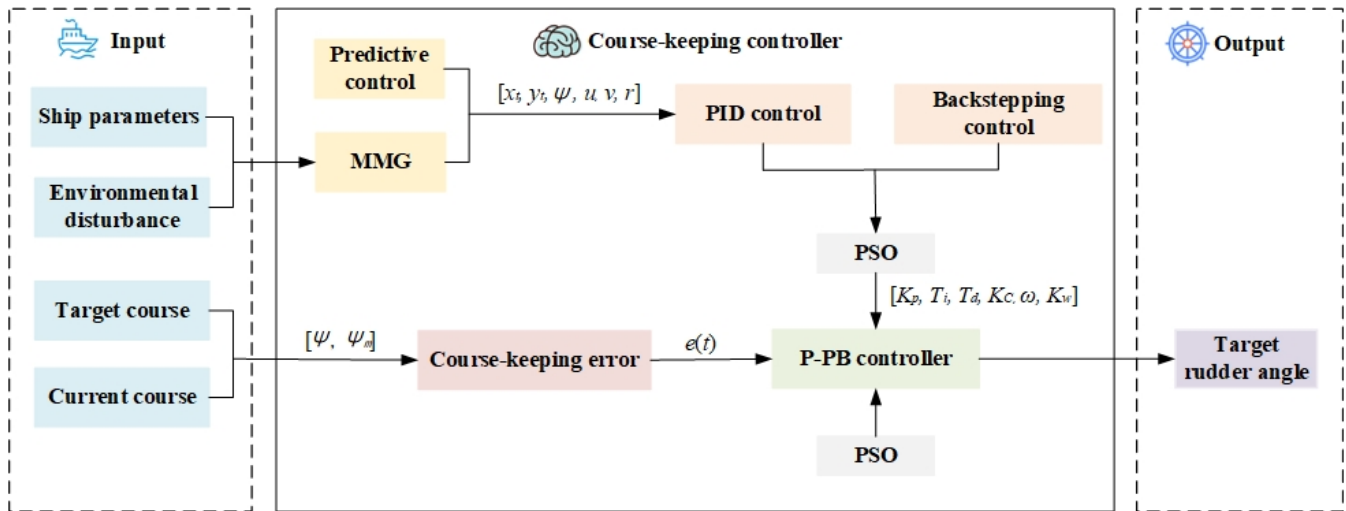

Figure 3. Framework of the P-PB course-keeping controller.

The inputs and outputs are defined first in order to design the course-keeping controller. The main principle of a course-keeping controller is to minimize course-keeping error by adjusting the rudder angle. Therefore, course-keeping error and target rudder angle are selected as the input and output of the proposed controller, respectively.

The course-keeping error is expressed in Equation (8),

$$e(t) = \psi_m - \psi \tag{8}$$

where $e(t)$ is the course-keeping error in time t, and ψ_m is the target course.

Then, the improved PID controller and the backstepping controller are combined to design the P-PB controller.

2.2.1. Improved PID Controller

PID control is a simple and reliable method that is widely adopted in the motion control of ships [22]. The basic formulation of the PID controller can be expressed as Equation (9),

$$u(t) = K_P[e(t) + \int_0^t e(t)\mathrm{dt}/T_i + T_d(\mathrm{de(t)/dt})] \tag{9}$$

where $u(t)$ is the output of the PID controller. K_P, T_i, and T_d are the proportional parameter, integral parameter, and derivative parameter, respectively.

To integrate the PID controller with the ship's rudder control, Equation (9) is modified as Equation (10):

$$\delta_E = \delta + K_P[e(t) + \int_0^t e(t)\mathrm{dt}/T_i + T_d(\mathrm{de(t)/dt})] \tag{10}$$

Then, to prevent control overshooting caused by the delayed ship motion, the PID controller is improved by introducing predictive control based on the MMG model [5,48].

Synthesizing the simplicity and interpretation of the controller, the improved PID controller is expressed as Equation (11),

$$\begin{cases} \delta_{EP} = \delta + K_P[e(t_{x3}) + \int_0^t e(t_{x3})dt/T_i + T_d(de(t_{x3})/dt)] \\ \quad -K_P[e(t_{x2}) + \int_0^t e(t_{x2})dt/T_i + T_d(de(t_{x2})/dt)] \quad\quad e(t_{x3}) > c_{f2}e(t_0) \\ \quad +K_P[e(t_{x1}) + \int_0^t e(t_{x1})dt/T_i + T_d(de(t_{x1})/dt)] \\ \delta_{EP} = \delta + c_{f1}K_P[e(t_{x3}) + \int_0^t e(t_{x3})dt/T_i + T_d(de(t_{x3})/dt)] \\ \quad -c_{f1}K_P[e(t_{x2}) + \int_0^t e(t_{x2})dt/T_i + T_d(de(t_{x2})/dt)] \quad c_{f2}e(t_0) > e(t_{x3}) > c_{f3}e(t_0) \\ \quad +c_{f1}K_P[e(t_{x1}) + \int_0^t e(t_{x1})dt/T_i + T_d(de(t_{x1})/dt)] \\ \delta_{EP} = 0 \quad\quad\quad\quad\quad\quad\quad\quad\quad\quad\quad\quad\quad e(t_{x3}) < c_{f3}e(t_0) \end{cases} \quad (11)$$

where δ_{EP} is the target rudder angle calculated by the improved PID controller, $e(t_x)$ is the course-keeping error predicted by the MMG model after x seconds, and c_f is the control factor with a value between 0 and 1.

2.2.2. Backstepping Controller

The formula of the backstepping controller is expressed as Equation (12),

$$\begin{cases} u_{BS} = m_{BS}\ddot{x}_{BS} + c_{BS}\dot{x}_{BS} + d_{BS} \\ y_{BS} = x_{BS} \end{cases} \quad (12)$$

where m_{BS}, c_{BS}, and d_{BS} are the variable parameters, u_{BS} is the input of the controller, and y_{BS} is the output of the backstepping controller.

Using the set $x_{1,BS} = x_{BS}$, $x_{2,BS} = \dot{x}_{BS}$, Equation (12) can be changed to Equation (13).

$$\begin{cases} \dot{x}_{1,BS} = x_{2,BS} \\ \dot{x}_{2,BS} = 1/m_{BS}(u_{BS} - c_{BS}x_{2,BS} - d_{BS}) \\ y_{BS} = x_{1,BS} \end{cases} \quad (13)$$

Next, the systematic error $z_{1,BS}$ is calculated.

$$z_{1,BS} = y_{BS} - y_{d,BS} \quad (14)$$

where $y_{d,BS}$ is the desired output.

Subsequently, the Lyapunov function $V_{1,BS}$ is defined in Equation (15).

$$V_{1,BS} = z_{1,BS}^2/2 \quad (15)$$

Then, the first order derivative of $V_{1,BS}$ can be expressed as Equation (16).

$$\dot{V}_{1,BS} = z_{1,BS}\dot{z}_{1,BS} = z_{1,BS}(\dot{y}_{BS} - \dot{y}_{d,BS}) \quad (16)$$

Consequently, the virtual control volume $a_{1,BS}$ is introduced to make $\dot{V}_{1,BS} \leq 0$.

$$a_{1,BS} = -\lambda_{1,BS}z_{1,BS} + \dot{y}_{d,BS} \quad (17)$$

where $\lambda_{1,BS} \geq 0$ is the constant.

After that, the error variable is defined.

$$z_{2,BS} = \dot{y}_{BS} - a_{1,BS} = \dot{x}_{1,BS} - a_{1,BS} = x_{2,BS} - a_{1,BS} \quad (18)$$

Substituting Equations (17) and (18) into Equation (16), the value of $\dot{V}_{1,BS}$ is expressed as Equation (19).

$$\dot{V}_{1,BS} = z_{1,BS}\dot{z}_{1,BS} = z_{1,BS}(z_{2,BS} + a_{1,BS} - \dot{y}_{d,BS}) = z_{1,BS}z_{2,BS} - \lambda_{1,BS}z_{1,BS}^2 \quad (19)$$

Then, set the Lyapunov function $V_{2,BS}$ as Equation (20).

$$\dot{V}_{2,BS} = \dot{V}_{1,BS} + z_{1,BS}z_{2,BS} = z_{1,BS}z_{2,BS} \\ - \lambda_{1,BS}z_{1,BS}^2 + z_{2,BS}[(u_{BS} - c_{BS}x_{2,BS} - d_{BS})/m - \dot{a}_{1,BS}] \tag{20}$$

Thus, the first order derivative of $V_{2,BS}$ can be calculated as Equation (21).

$$\dot{V}_{2,BS} = z_{1,BS}z_{2,BS} - \lambda_{1,BS}z_{1,BS}^2 + z_{2,BS}[(u_{BS} - c_{BS}x_{2,BS} - d_{BS})/m - \dot{a}_{1,BS}] \\ = -(\lambda_{1,BS}z_{1,BS}^2 + \lambda_{2,BS}z_{2,BS}^2) \tag{21}$$

Finally, the backstepping control law u_{BS} is determined using Equation (22).

$$u_{BS} = m_{BS}(\dot{a}_{1,BS} - \lambda_{2,BS}z_{2,BS} - z_{1,BS}) + c_{BS}x_{2,BS} + d_{BS} \tag{22}$$

By combining the backstepping controller with the rudder control, the improved backstepping controller for the course-keeping of the ship [9] is shown in Equation (23),

$$\begin{cases} H(r) = (\alpha + \beta)r \\ b = K/T \\ \delta_{EB} = 1/b[-bH(r) + K_C \sin(\omega e(t))] \end{cases} \tag{23}$$

where α, β, K, and T are the ship's maneuvering indexes, which can be determined in Ref [51]. K_C and ω are the variable parameters of the controller. δ_{EB} is the target rudder angle calculated by the improved backstepping controller.

The backstepping controller has the advantage of a shorter time required to approach the target course, but its course-keeping stability is relatively poor [25]. Meanwhile, it is less accurate under harsh environmental disturbances affected by the dependence of r.

2.2.3. Design of the P-PB Controller

The improved PID and backstepping controller are combined to establish the P-PB controller. The main control law of the P-PB controller is designed using Equation (24),

$$\delta_{PPB} = K_w \delta_{EP} + (1 - K_w)\delta_{EB} \tag{24}$$

where δ_{PPB} is the target rudder angle calculated by the proposed P-PB controller. K_w is the control factor, with a value between 0 and 1.

By changing the value of K_w, the weights of the improved PID and backstepping controllers can be adjusted adaptively. Therefore, the P-PB controller combines the features of both controllers to achieve better control efficiency in various scenarios.

2.3. Parameter Optimization of the Ship Course-Keeping Controller

PSO was presented by Kennedy and R. Eberhart in 1994 and it is adopted as an effective approach to solving dynamic and multi-objective optimizing problems [52]. Therefore, PSO is adopted to optimize parameters in the proposed P-PB controller. The flowchart for optimizing the parameters of the proposed P-PB course-keeping controller is shown in Figure 4.

The values of K_P, T_i, T_d, K_C, ω, and K_w are defined as the key parameters to be optimized. To generate the particle swarm for each parameter, the population size of PSO is set as N, the learning factors are set as $c1$ and $c2$. The inertia weight value is set as w, and the maximum iteration number is set as T.

After initializing the population, the initial position (value) of each parameter $x_{PSO} = [K_P, T_i, T_d, K_C, \omega, K_w]$ and velocity v_{PSO} of the particle group is generated, which makes up the initial particle.
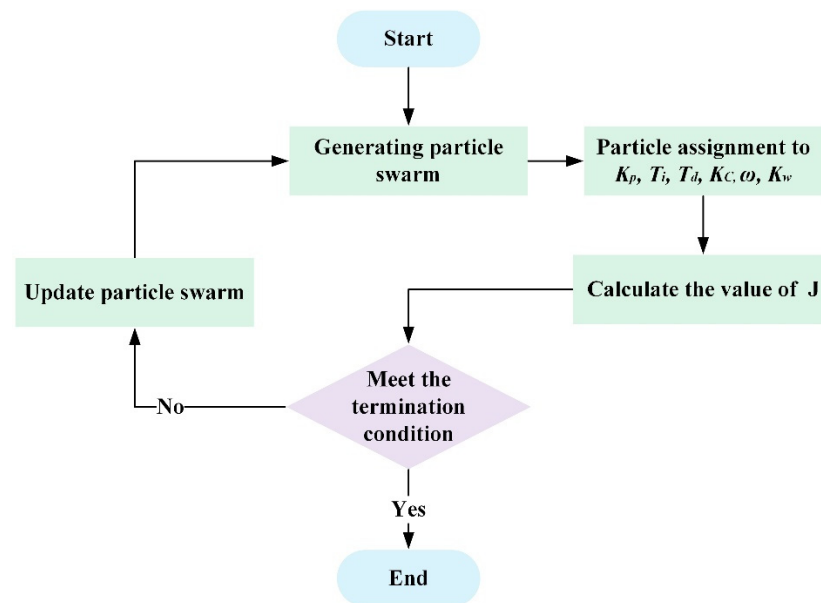
Figure 4. Flowchart of course-keeping controller parameter optimization.

Subsequently, the fitness function is defined to calculate the fitness value of each particle using Equation (25):

$$J = 1/\sum_{s=1}^{step} (\psi_m - \psi) \tag{25}$$

where J is the fitness value, and $step$ is the time duration of the optimization.

By using the MMG model to predict the ship's motion state, the value of J is determined when adopting the current parameters.

Subsequently, more particles are generated and compared to find the maximum fitness value. The position and velocity of each particle which contains different values of the key parameters are updated as Equation (26). Then, the fitness value of each particle is compared with the historical optimal fitness value. Then, the global optimal position g and global optimal fitness value g_{best} are obtained:

$$\begin{cases} v_i^{k+1} = wv_i^k + r_1c_1(g - x_i^k) + r_2c_2(g_{best} - x_i^k) \\ x_i^{k+1} = x_i^k + v_i^{k+1} \end{cases} \tag{26}$$

where r_1, r_2 is a random value between 0 and 1, and i is the current particle number.

Finally, the value of each parameter can be continuously optimized until it meets the termination condition, and the value of key parameters with the max fitness value can be achieved.

## 3. Application of the P-PB Ship Course-Keeping Controller

3.1. Simulation Preliminaries

A ship named KVLCC2 is selected as the case ship to verify the effectiveness of the P-PB controller. The main parameters of KVLCC2 are shown in Table 1, other parameters are shown in Ref [53].

After establishing the nonlinear ship model of KVLCC2 in Section 2.1, the simulation results of the turning test, with an initial ship speed of 15.5 kn/h, rudder angle of $\pm 35°$, and initial course of $0°$, are compared with the results of Yasukawa and Yoshimura [53]. A comparison of ship's trajectory is shown in Figure 5.

Table 1. Parameters of KVLCC2.

Parameter	Value	Unit
Length	320	m
Breadth	58	m
Draft	20.8	m
Displacement	312,622	m^3
Open water speed	15.5	kn/h
Initial course	0	deg
Max steering speed of rudder	2.34	deg/s
Max rudder angle	35	deg
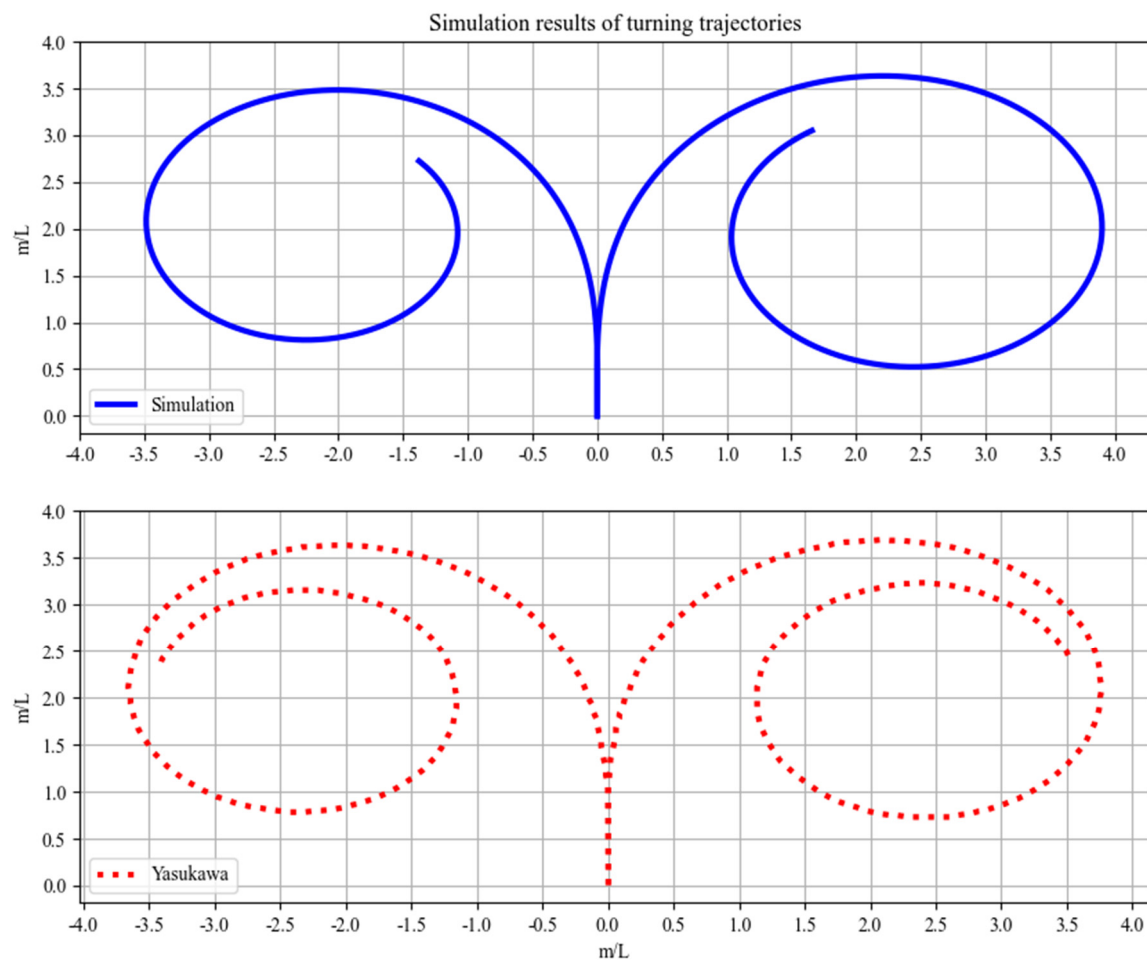
Figure 5. Comparison of ship trajectory; Yasukawa & Yoshimura, 2015 [53].

The accuracy of the ship's turning test can be verified using the formula below [54]:

$$C_M = \frac{\min(S_D, R_D)}{\max(S_D, R_D)} 100\% \tag{27}$$

where S_D is the simulation result, R_D is the experimental result, and C_M is the consistency evaluation indicator.

Finally, a comparison of the ship's turning test is shown in Table 2. The consistency between simulation results in this study and Yasukawa [53] is 97.52%. The simulation results are in line with the valid experimental results.

Table 2. Comparison of simulation results.

Turning Test	$A_d/L(\delta = 35°)$	$T_d/L(\delta = 35°)$	$A_d/L(\delta = -35°)$	$T_d/L(\delta = -35°)$
Yasukawa & Yoshimura (2015) [53]	3.67	3.71	3.56	3.59
Simulation	3.64	3.90	3.49	3.49
C_M	99.18%	95.13%	98.03%	97.72%
$\overline{C}_M$		97.52%		

A_d and T_d are the advance and tactical diameter of the turning test, respectively.

To verify the efficiency of the P-PB controller under various environmental disturbances, simulation scenarios were established, as described in Table 3.

**Table 3.** Simulation scenarios for the course-keeping test.

Simulation Scenario	Wind Speed (m/s)	Wind Direction (°)	Target Course (°)			
			0–900 s	900–1800 s	1800–2700 s	2700–3600 s
No wind	0	/	30	10	−5	20
Low speed wind	10	30	30	10	−5	20
High speed wind	20	30	30	10	−5	20

Then, to balance the efficiency and accuracy of PSO when optimizing the P-PB controller, the main parameters of PSO were set, as described in Table 4.

Table 4. Main parameters of PSO.

Parameter	Value
N	20
T	40
$c1$	2
$c2$	2
w	0.5

The change curve of the fitness value for iterations under each stage is shown in Figure 6. The fitness value increased with each iteration and eventually stabilized in each stage, which ensured the effectiveness and completeness of the optimization.
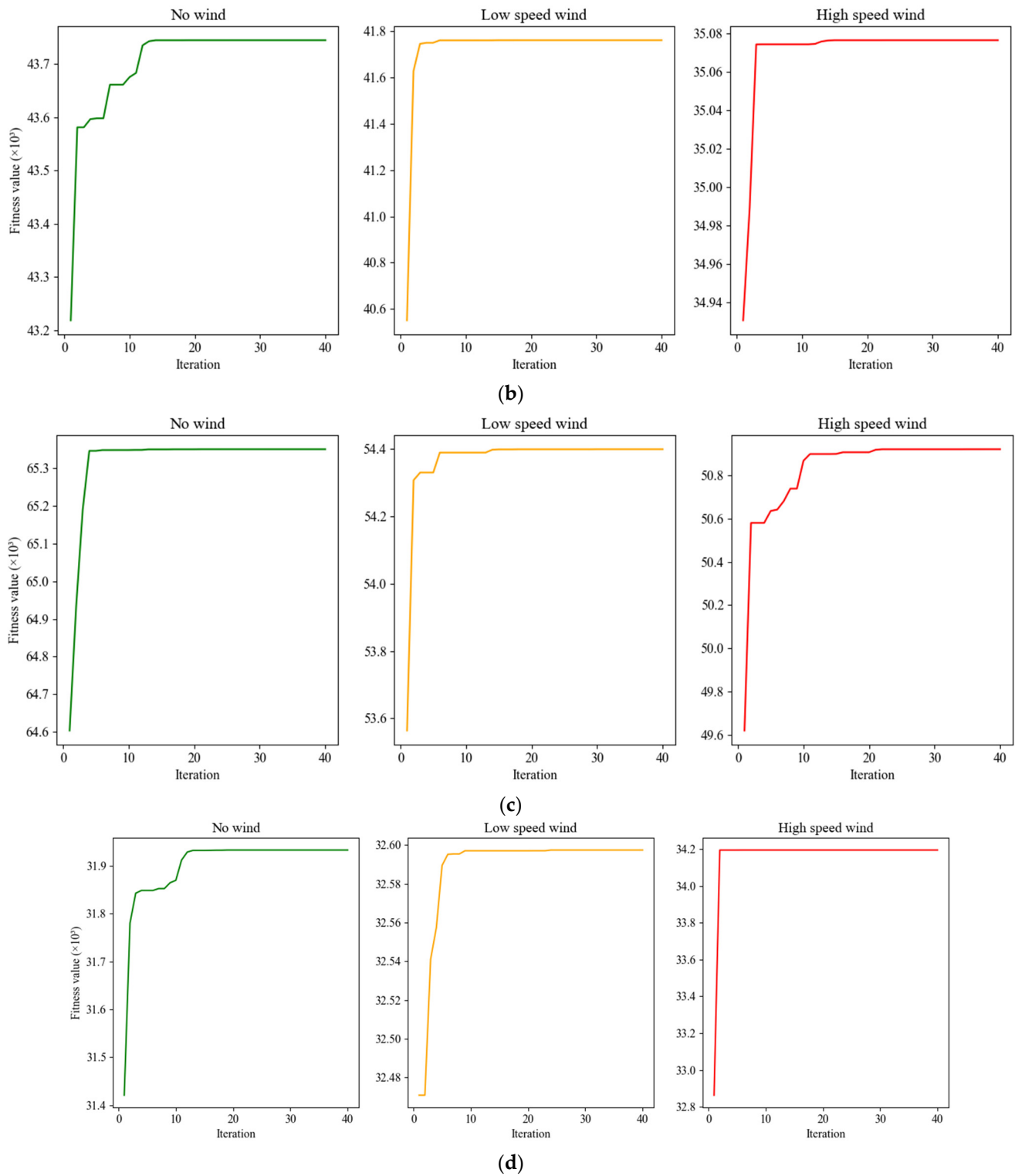

(a)

Figure 6. *Cont.*

(b)

(c)

(d)
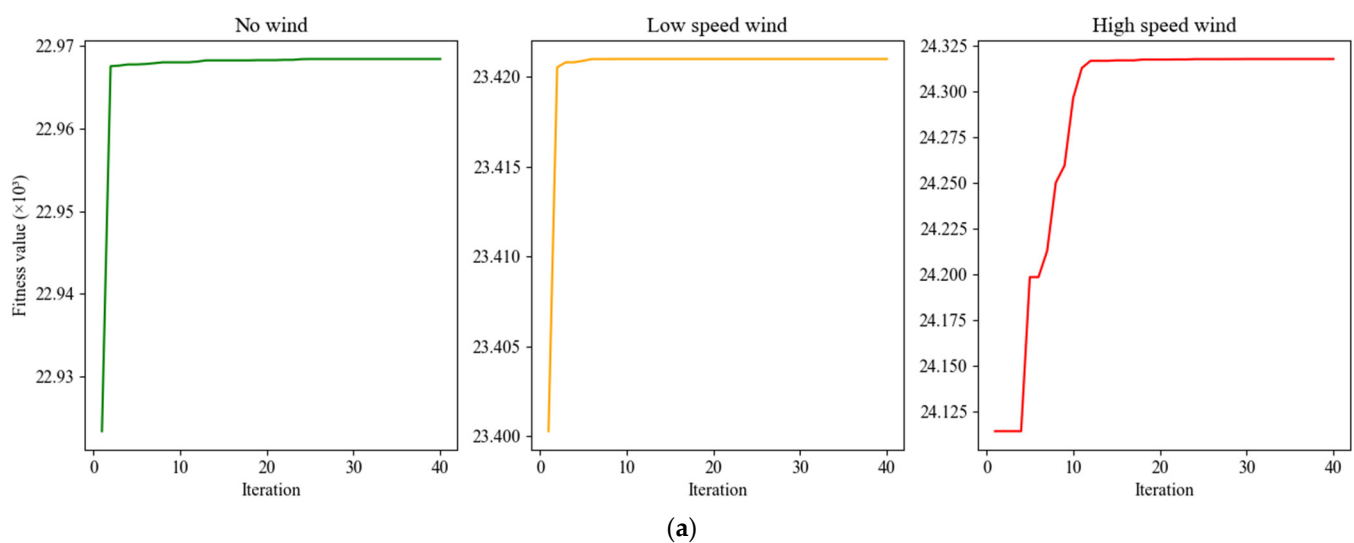
Figure 6. Change curves of fitness values for iterations in (**a**) 0–900, (**b**) 900–1800, (**c**) 1800–2700, and (**d**) 2700–3600 s.

*3.2. Comparison and Analysis of Simulation Results*

The P-PB controller was valid when compared to the improved PID controllers proposed by Diabac and He [22,23] and the controller based on backstepping control proposed by Zhang [9]. The change in ship's course under these three models and the proposed P-PB controller is compared in various scenarios, as shown in Figure 7.
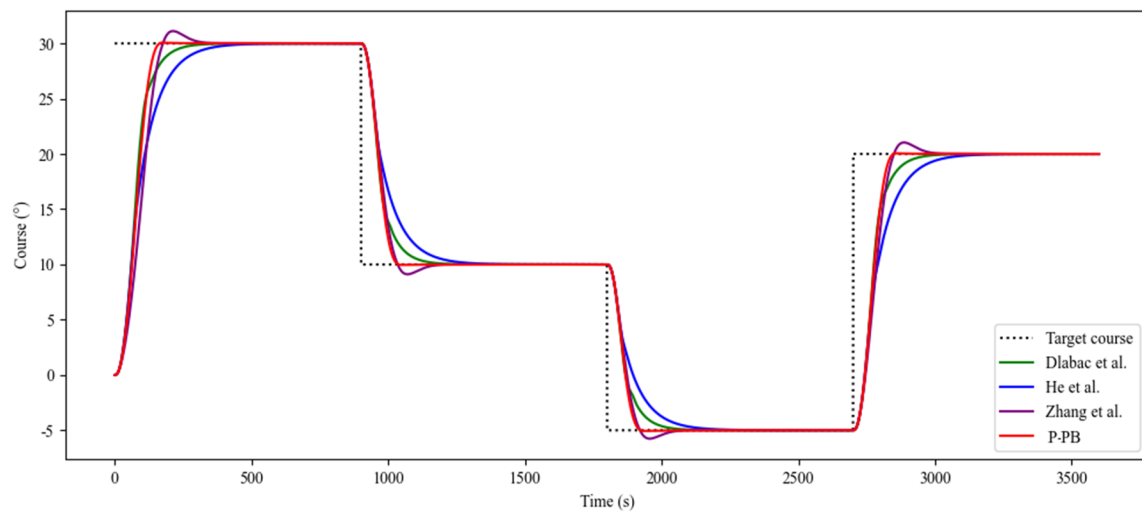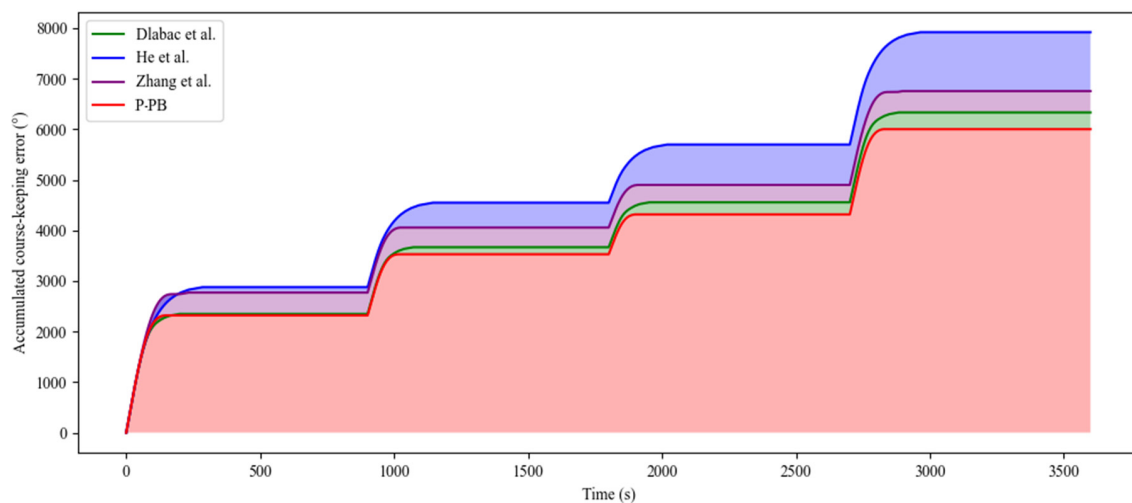
(**a**)
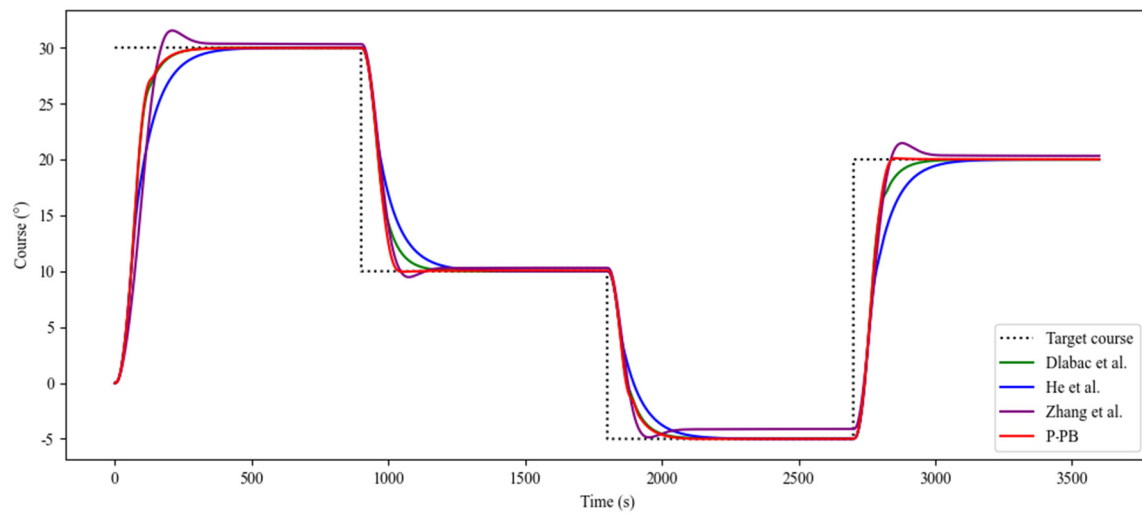
(**b**)
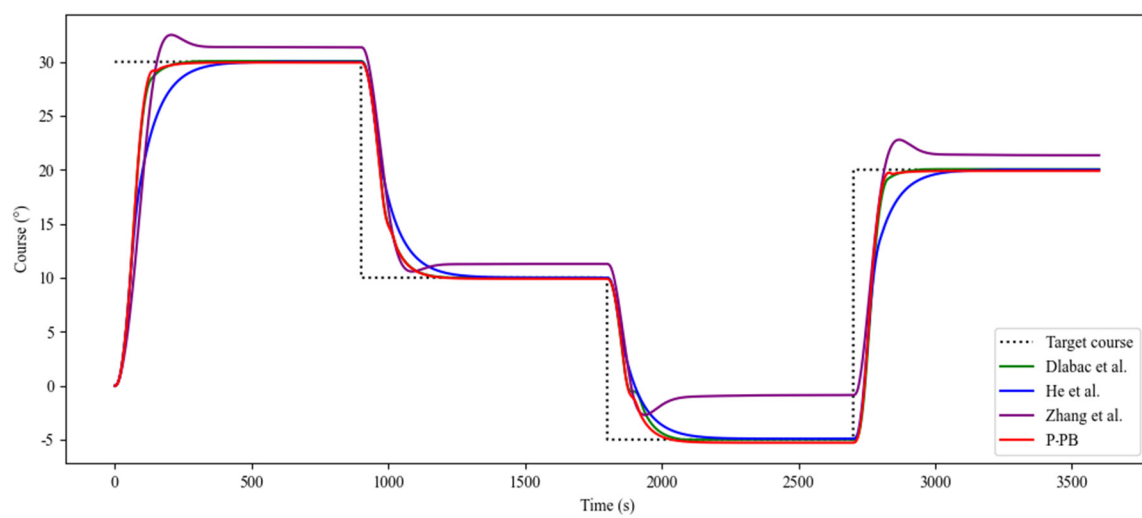
(**c**)

Figure 7. Comparison of the ship's course under (**a**) no wind, (**b**) low-speed wind, and (**c**) high-speed wind scenarios; Dlabac et al. (2019) [22], He et al. (2020) [23], Zhang et al. (2020) [24].

As seen in Figure 7, all the controllers kept the ship on course under various environmental disturbances. When comparing the four controllers, it is obvious that the P-PB controller and the controller proposed by Dlabac [22] and Zhang [24] responded more quickly and tracked the target course satisfactorily in the initial stage when the target course was changing.

However, the overshoot of the backstepping controller proposed by Zhang [24] increased rapidly as the environmental disturbances became harsher. This is because the yawing speed of the ship is considered one of the inputs of the improved backstepping controller proposed by Zhang [24]. When an environmental disturbance is lower, consideration of the ship's yawing speed is an effective way to improve the stability and accuracy of the course-keeping controller. Conversely, when an environmental disturbance is larger, external factors significantly interfere with the ship's yawing speed, which causes the ship's course-keeping error to increase rapidly.

The proposed P-PB controller also considers the ship's yawing speed to achieve efficient course-keeping control when environmental disturbances are lower. Furthermore, when environmental disturbances gradually increase, an overshoot of ship course-keeping is avoided by adjusting the value of K_w using PSO. Therefore, a smaller course-keeping error can be obtained under various scenarios.

The accumulated course-keeping error is compared in Figure 8.
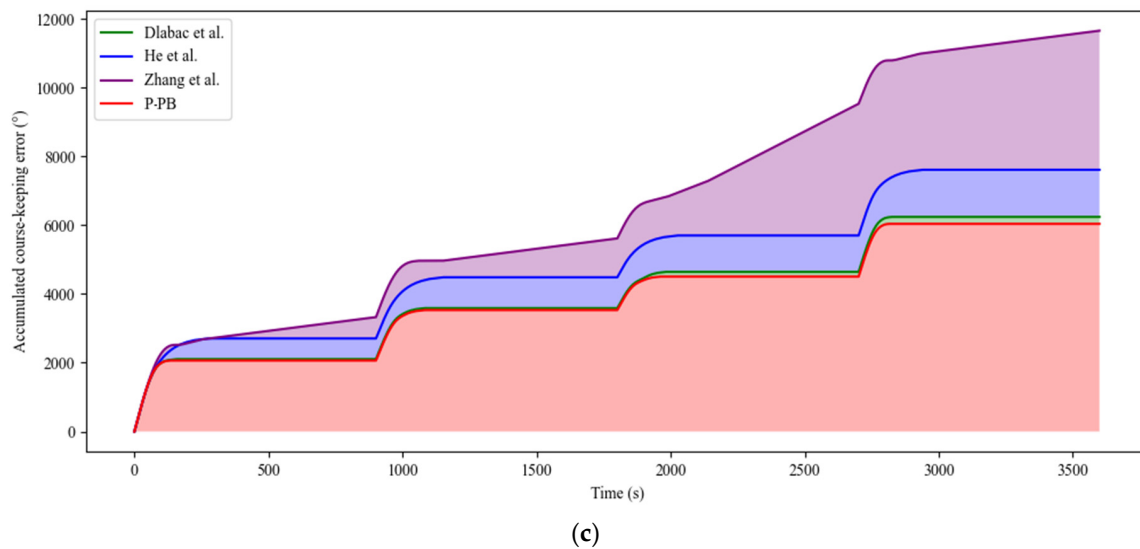
(**a**)

(**b**)

Figure 8. *Cont.*

(c)
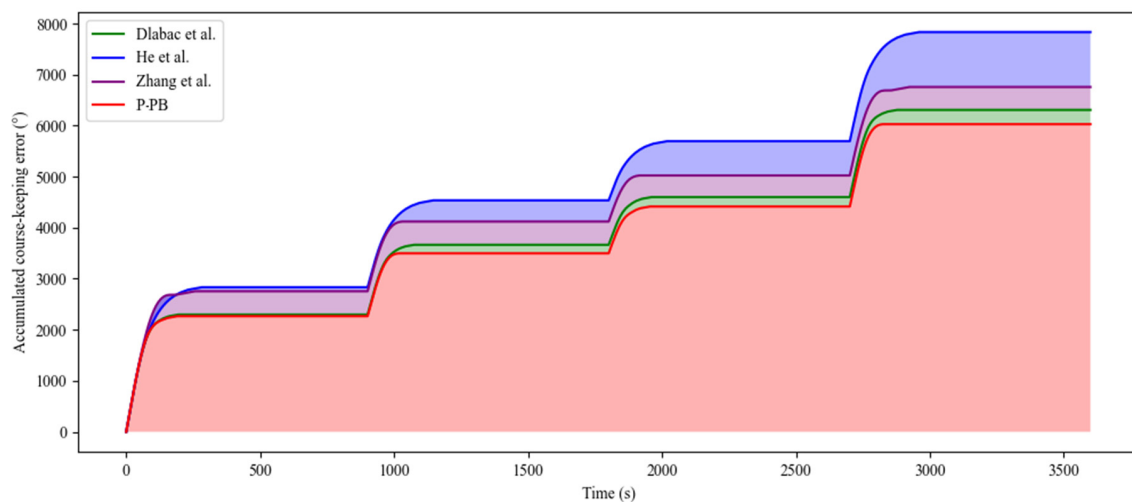
Figure 8. Comparison of the accumulated course-keeping error under (**a**) no wind, (**b**) low-speed wind, and (**c**) high-speed wind scenarios; Dlabac et al. (2019) [22], He et al. (2020) [23], Zhang et al. (2020) [24].

The mean course-keeping error, which is calculated by dividing the accumulated course-keeping error by time, is shown in Figure 9. It illustrates the mean course-keeping error for each controller as a percentage of the accumulated mean course-keeping error for the four controllers, and each circle represents one percent. For example, when under a high-speed wind scenario, the accumulated mean course-keeping error of the four controllers is $8.77°$, and the mean course-keeping error of the P-PB controller is $1.67°$, which accounts for 19.04% of the mean course-keeping error and therefore occupies 19 circles.
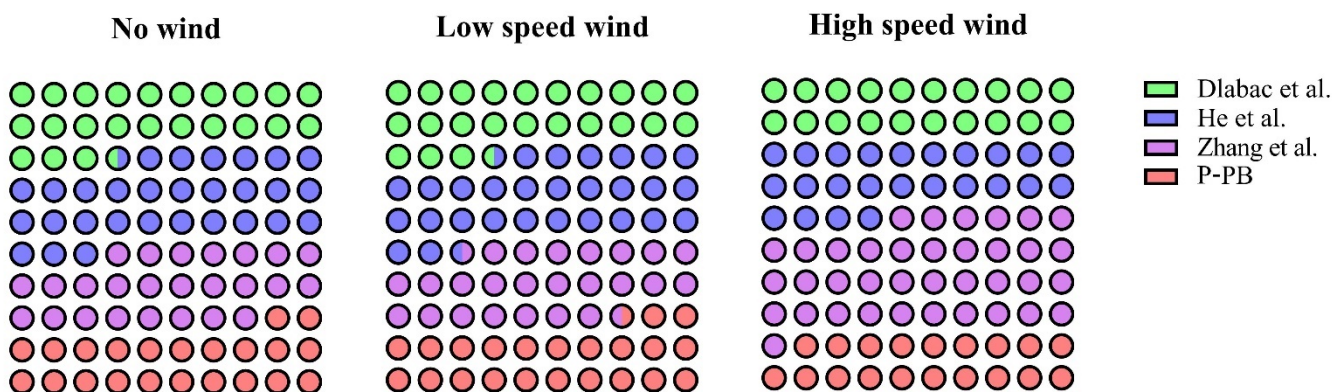

Figure 9. Comparison of the mean course-keeping error; Dlabac et al. (2019) [22], He et al. (2020) [23], Zhang et al. (2020) [24].

The smaller the number of circles corresponding to the controllers, the smaller the average error of the controllers compared to the other controllers, and therefore the more efficient the controller is.

As indicated by Figures 7–9, it is clear that the P-PB controller and the controller proposed by Dlabac [22] achieved course-keeping with the lowest and second-lowest accumulated course-keeping error, respectively, throughout the simulation tests under the three scenarios. Meanwhile, compared to the controller proposed by Dlabac [22], the P-PB controller had a larger advantage in terms of accumulated course-keeping error when environmental disturbances were lower.

The accumulated course-keeping error of the controller proposed by Zhang [24] performed better under lower environmental disturbances. However, its accumulated

course-keeping error increased significantly under extreme environmental disturbances. The improved PID controller proposed by He performed stably in various scenarios, but was slightly slower to reach the target course.

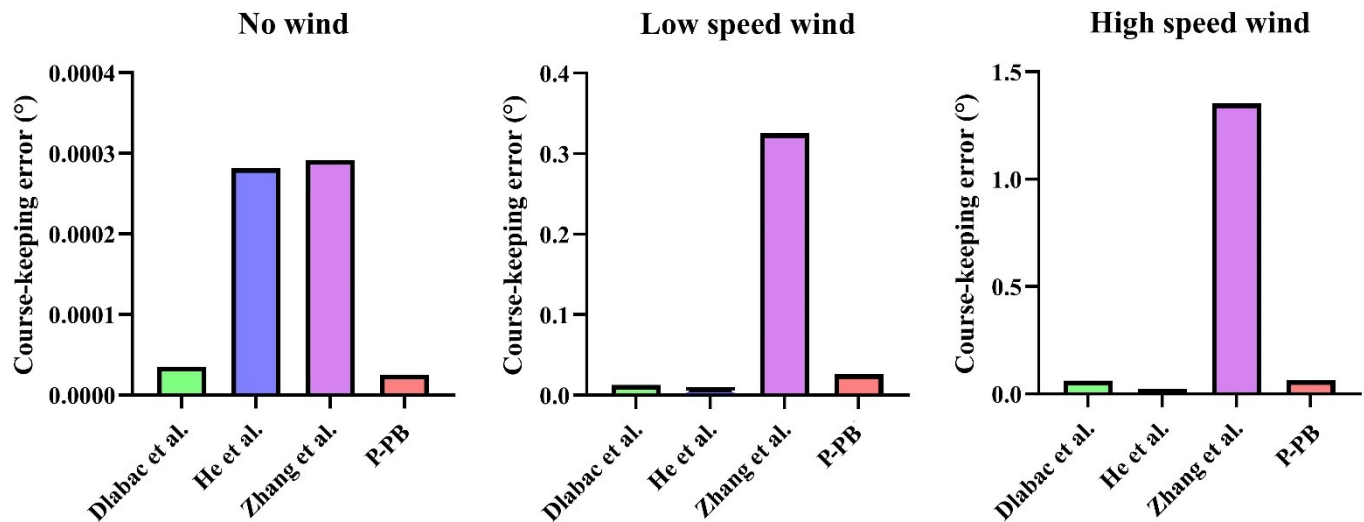The course-keeping error when the ship's course is stabilized is shown in Figure 10.

Figure 10. Comparison of the stabilized course-keeping error; Dlabac et al. (2019) [22], He et al. (2020) [23], Zhang et al. (2020) [24].

When there was no environmental disturbance, the stabilized course-keeping error of all four controllers was extremely small. Among them, the controller proposed by Dlabac [22] and the P-PB controller had the lowest stabilized course-keeping error. However, with the gradual increase in environmental disturbances, the course-keeping error of Zhang's [24] proposed controller increased rapidly, and the errors of the P-PB and Dlabac's [22] proposed controllers also increased. He's proposed controller maintained a lower error than the other controllers under environmental disturbances.

The average rudder angle in the various scenarios is shown in Figure 11. The average rudder angles of all ship course-keeping controllers increased when the wind disturbance became harsher.
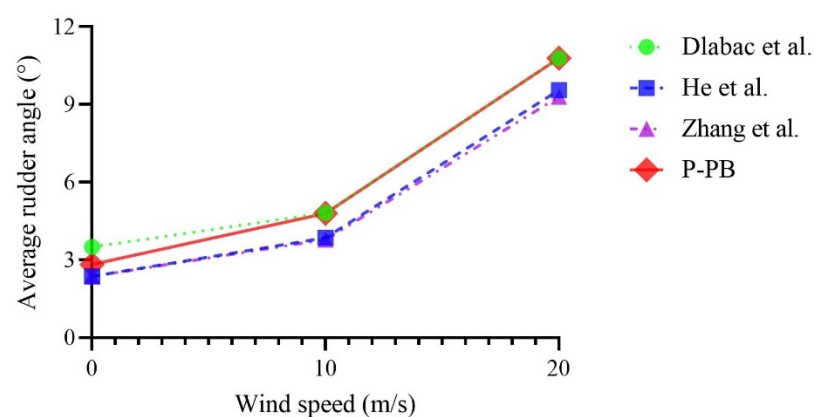

Figure 11. Comparison of average rudder angle; Dlabac et al. (2019) [22], He et al. (2020) [23], Zhang et al. (2020) [24].

When comparing the four controllers, the controllers proposed by Zhang [24] and He [23] achieved course-keeping with a smaller rudder angle under all scenarios. Conversely, the P-PB controller and the controller proposed by Dlabac [22] had a larger average rudder angle and therefore required relatively more energy for control. Furthermore, when comparing the above-two controllers with lower course-keeping errors,

the P-PB controller had a relatively small average rudder angle, especially under lower environmental disturbances.

Finally, the mean course-keeping error for the four controllers is shown in Table 5. Compared to other controllers, the P-PB controller improved course-keeping error by 4.19% on average.

Table 5. Course-keeping controller performance.

Course-Keeping Controller	Mean Course-Keeping Error (°)		
	No Wind	**Low Speed Wind**	**High Speed Wind**
Dlabac et al. [22]	1.76	1.75	1.73
He et al. [23]	2.20	2.18	2.12
Zhang et al. [24]	1.88	1.88	3.23
P-PB	1.67	1.67	1.68
Improvement	5.11%	4.57%	2.89%
Average improvement		4.19%	

When environmental disturbances increased, the reduction in the ship course-keeping error of some controllers was due the fact that the disturbance matched the direction of the ship's course, and therefore the ship achieved the target course in a shorter period of time.

To provide a comprehensive analysis of the control effectiveness of the P-PB controller, time-response specifications have been compared. Among them, rise time is the time required to adjust the ship's course to 90% of the target course, which represents the rapidity of the controller's response. Overshoot characterizes the maximum deviation of the controller, and the smaller its value the better the stability of the controller. Settling time refers to the time it takes to maintain a course-keeping error within 2% and is a key factor of control stability. The mean value of each specification in the various scenarios is shown in Table 6.

Table 6. Comparison of time response specifications.

Course-Keeping Controller	Time-Response Specification		
	Rise Time (s)	**Settling Time (s)**	**Overshoot (%)**
Dlabac et al. [22]	134.83	209.92	0.01
He et al. [23]	191.17	312.17	0.01
Zhang et al. [24]	186.67	195.77	5.35
P-PB	117.42	158.17	0.16
Improvement	12.91%	19.21%	−2.99%
Average improvement		9.71%	

As seen in Table 6, the proposed P-PB controller saw a 9.71% improvement on average in terms of time-response specification. Analyzing the time-response specification, the proposed controller has a faster response speed and better control stability compared to the other controllers, providing further confirmation of the controller's effectiveness. However, some overshoot remains. This is attributed to the fact that the PSO-optimized controller retains a partial dependence on *r* to reduce the course-keeping error.

In summary, the P-PB controller proposed in this paper can realize a stabilized course-keeping of ships with lower error and better time-response performance, providing a new approach for the automatic control of ships.

4. Conclusions

This study proposes a PSO-based predictive PID-backstepping controller for the course-keeping of ships, taking target course, current course, yawing speed, and predictive motion parameters into consideration. The proposed controller is designed based on the predictive PID controller and backstepping controller. The parameters in the proposed

controller are optimized via PSO. Finally, the proposed controller's efficacy was demonstrated by comparing it with other ship controllers in various scenarios. Comparison results illustrate that the proposed controller can achieve the target course more quickly and more precisely under various environmental disturbances, which provides a new approach for the course-keeping of ships. However, the proposed method has a larger average rudder angle, which may lead to higher energy consumption. In future research, improvements can be made to improve energy consumption in ship course-keeping.

Although the research in this study revealed some important findings, there are still some limitations that need to be further researched in the future. Firstly, the hydrodynamic coefficients in this paper were mainly calculated using empirical formulas, which could be further optimized to improve the accuracy of the ship motion model. Second, the current study does not consider the effect of obstacles on course-keeping during navigation.

Author Contributions: All authors contributed to this study. B.L.: Conceptualization, Methodology, Software, Visualization, Writing—original draft, Writing—review & editing; M.Z. (Mao Zheng): Conceptualization, Data curation, Funding acquisition, Investigation, Supervision, Validation, Writing—review & editing; B.H.: Investigation, Conceptualization, Project administration, Supervision, Validation, Writing—original draft, Writing—review & editing; X.C.: Conceptualization, Data curation, Formal analysis, Funding acquisition, Investigation, Project administration, Writing—review & editing; M.Z. (Mingyang Zhang): Supervision, Validation, Writing—original draft, Writing—review & editing; H.Z. and S.D.: Software, Writing—review & editing; H.W. and K.Z.: Writing—review & editing. All authors have read and agreed to the published version of the manuscript.

Institutional Review Board Statement: Not applicable.

Informed Consent Statement: Not applicable.

Data Availability Statement: Data are contained within the article.

Conflicts of Interest: The authors declare no conflict of interest.

References

1. Sun, Y.; Lu, Z.; Lian, F.; Yang, Z. Study of Channel Upgrades and Ship Choices of River-Shipping of Port Access-Transportation. *Transp. Res. Part Transp. Environ.* **2023**, *119*, 103733. [CrossRef]
2. Liu, Z.; Gao, H.; Zhang, M.; Yan, R.; Liu, J. A Data Mining Method to Extract Traffic Network for Maritime Transport Management. *Ocean Coast. Manag.* **2023**, *239*, 106622. [CrossRef]
3. Clark, X.; Dollar, D.; Micco, A. Port Efficiency, Maritime Transport Costs, and Bilateral Trade. *J. Dev. Econ.* **2004**, *75*, 417–450. [CrossRef]
4. Grewal, D.; Haugstetter, H. Capturing and Sharing Knowledge in Supply Chains in the Maritime Transport Sector: Critical Issues. *Marit. Policy Manag.* **2007**, *34*, 169–183. [CrossRef]
5. Ma, D.; Chen, X.; Ma, W.; Zheng, H.; Qu, F. Neural Network Model-Based Reinforcement Learning Control for AUV 3-D Path Following. *IEEE Trans. Intell. Veh.* **2023**, 1–13. [CrossRef]
6. He, Z.; Liu, C.; Chu, X.; Negenborn, R.R.; Wu, Q. Dynamic Anti-Collision A-Star Algorithm for Multi-Ship Encounter Situa-tions. *Appl. Ocean Res.* **2022**, *118*, 102995. [CrossRef]
7. Chu, Z.; Yan, R.; Wang, S. Evaluation and Prediction of Punctuality of Vessel Arrival at Port: A Case Study of Hong Kong. *Marit. Policy Manag.* **2023**, 1–29. [CrossRef]
8. Lin, B.; Zheng, M.; Chu, X.; Zhang, M.; Mao, W.; Wu, D. A Novel Method for the Evaluation of Ship Berthing Risk Using AIS Data. *Ocean Eng.* **2024**, *293*, 116595. [CrossRef]
9. Zhang, Q.; Zhang, M.; Hu, Y.; Zhu, G. Error-Driven-Based Adaptive Nonlinear Feedback Control of Course-Keeping for Ships. *J. Mar. Sci. Technol.* **2021**, *26*, 357–367. [CrossRef]
10. Zhang, M.; Conti, F.; Le Sourne, H.; Vassalos, D.; Kujala, P.; Lindroth, D.; Hirdaris, S. A Method for the Direct Assessment of Ship Collision Damage and Flooding Risk in Real Conditions. *Ocean Eng.* **2021**, *237*, 109605. [CrossRef]
11. Zhang, M.; Taimuri, G.; Zhang, J.; Hirdaris, S. A Deep Learning Method for the Prediction of 6-DoF Ship Motions in Real Conditions. *Proc. Inst. Mech. Eng. Part M J. Eng. Marit. Environ.* **2023**, *237*, 887–905. [CrossRef]
12. Liu, Z.; Zhang, B.; Zhang, M.; Wang, H.; Fu, X. A Quantitative Method for the Analysis of Ship Collision Risk Using AIS Data. *Ocean Eng.* **2023**, *272*, 113906. [CrossRef]

13. Zhang, M.; Kujala, P.; Musharraf, M.; Zhang, J.; Hirdaris, S. A Machine Learning Method for the Prediction of Ship Motion Trajectories in Real Operational Conditions. *Ocean Eng.* **2023**, *283*, 114905. [CrossRef]
14. Lin, B.; Zheng, M.; Chu, X.; Mao, W.; Zhang, D.; Zhang, M. An Overview of Scholarly Literature on Navigation Hazards in Arctic Shipping Routes. *Environ. Sci. Pollut. Res.* **2023**, 1–17. [CrossRef] [PubMed]
15. Min, B.; Zhang, X. Concise Robust Fuzzy Nonlinear Feedback Track Keeping Control for Ships Using Multi-Technique Improved LOS Guidance. *Ocean Eng.* **2021**, *224*, 108734. [CrossRef]
16. Kim, D.; Song, S.; Jeong, B.; Tezdogan, T.; Incecik, A. Unsteady RANS CFD Simulations of Ship Manoeuvrability and Course Keeping Control under Various Wave Height Conditions. *Appl. Ocean Res.* **2021**, *117*, 102940. [CrossRef]
17. Kim, D.; Tezdogan, T. CFD-Based Hydrodynamic Analyses of Ship Course Keeping Control and Turning Performance in Irregular Waves. *Ocean Eng.* **2022**, *248*, 110808. [CrossRef]
18. Liu, Z. Ship Adaptive Course Keeping Control With Nonlinear Disturbance Observer. *IEEE Access* **2017**, *5*, 17567–17575. [CrossRef]
19. Liu, Z. Ship Course Keeping Using Different Sliding Mode Controllers. *Trans. Famena* **2019**, *43*, 49–60. [CrossRef]
20. Liangqi, L.; Renxiang, B.; Wuchen, S.; Xinyu, L. Ship Track-Keeping Control Based on Sliding Mode Variable Structure PID Controller and Particle Swarm Optimization. In Proceedings of the 2019 6th International Conference on Information Science and Control Engineering (ICISCE), Shanghai, China, 20–22 December 2019; pp. 887–891.
21. Islam, M.M.; Siffat, S.A.; Ahmad, I.; Liaquat, M. Supertwisting and Terminal Sliding Mode Control of Course Keeping for Ships by Using Particle Swarm Optimization. *Ocean Eng.* **2022**, *266*, 112942. [CrossRef]
22. Dlabač, T.; Ćalasan, M.; Krčum, M.; Marvučić, N. PSO-Based PID Controller Design for Ship Course-Keeping Autopilot. *Brodogradnja* **2019**, *70*, 1–15. [CrossRef]
23. He, Y.; Zhang, X.; Yu, Y.; Li, M.; Gong, S.; Jin, Y.; Mou, J. Ship Dynamic Collision Avoidance Mechanism Based on Course Control System. *Ournal Southwest Jiaotong Univ.* **2020**, *55*, 988–993+1027.
24. Zhang, Q.; Ding, Z.; Zhang, M. Adaptive Self-Regulation PID Control of Course-Keeping for Ships. *Pol. Marit. Res.* **2020**, *27*, 39–45. [CrossRef]
25. Wang, C.; Yan, C.; Liu, Z.; Cao, F. An Inverse Optimal Approach to Ship Course-Keeping Control. *IMA J. Math. Control Inf.* **2020**, *37*, 1192–1217. [CrossRef]
26. Islam, M.M.; Siffat, S.A.; Ahmad, I.; Liaquat, M. Robust Integral Backstepping and Terminal Synergetic Control of Course Keeping for Ships. *Ocean Eng.* **2021**, *221*, 108532. [CrossRef]
27. Hu, Y.; Su, W.; Zhang, Q.; Zhang, Y.; Wang, C. A Nonlinear Power Feedback Improvement of the Ship Course-Keeping Controller. *Math. Probl. Eng.* **2022**, *2022*, e3095122. [CrossRef]
28. Zhang, Q.; Zhang, X.; Im, N. Ship Nonlinear-Feedback Course Keeping Algorithm Based on MMG Model Driven by Bipolar Sigmoid Function for Berthing. *Int. J. Nav. Archit. Ocean Eng.* **2017**, *9*, 525–536. [CrossRef]
29. Min, B.; Zhang, X.; Wang, Q. Energy Saving of Course Keeping for Ships Using CGSA and Nonlinear Decoration. *IEEE Access* **2020**, *8*, 141622–141631. [CrossRef]
30. Borkowski, P. Inference Engine in an Intelligent Ship Course-Keeping System. *Comput. Intell. Neurosci.* **2017**, *2017*, e2561383. [CrossRef]
31. Zirilli, A.; Roberts, G.N.; Tiano, A.; Sutton, R. Adaptive Steering of a Containership Based on Neural Networks. *Int. J. Adapt. Control Signal Process.* **2000**, *14*, 849–873. [CrossRef]
32. Xu, H.-J.; Li, W.; Yu, Y.; Liu, Y. A Novel Adaptive Neural Control Scheme for Uncertain Ship Course-Keeping System. *Sens. Transducers* **2014**, *178*, 282.
33. Zhang, S.; Zhang, Q.; Su, W.; Li, H.; Gai, X. Ship Adaptive RBF Neural Network Course Keeping Control Considering System Uncertainty. In Proceedings of the 2023 IEEE 12th Data Driven Control and Learning Systems Conference (DDCLS), Xiangtan, China, 12–14 May 2023; pp. 1398–1403.
34. Wang, Q.; Sun, C.; Chen, Y. Adaptive Neural Network Control for Course-Keeping of Ships with Input Constraints. *Trans. Inst. Meas. Control* **2019**, *41*, 1010–1018. [CrossRef]
35. Le, T.T. Ship Heading Control System Using Neural Network. *J. Mar. Sci. Technol.* **2021**, *26*, 963–972. [CrossRef]
36. Zhang, Z.; Zhang, X.; Zhang, G. ANFIS-Based Course-Keeping Control for Ships Using Nonlinear Feedback Technique. *J. Mar. Sci. Technol.* **2019**, *24*, 1326–1333. [CrossRef]
37. Wang, C.; Yan, C.; Liu, Z. Leader-Following Consensus for Second-Order Nonlinear Multi-Agent Systems Under Markovian Switching Topologies with Application to Ship Course-Keeping. *Int. J. Control Autom. Syst.* **2021**, *19*, 54–62. [CrossRef]
38. Mohd Tumari, M.Z.; Zainal Abidin, A.F.; Hussin, M.S.F.; Abd Kadir, A.M.; Mohd Aras, M.S.; Ahmad, M.A. PSO Fine-Tuned Model-Free PID Controller with Derivative Filter for Depth Control of Hovering Autonomous Underwater Vehicle. In Proceedings of the 10th National Technical Seminar on Underwater System Technology, Pekan, Malaysia, 26–27 September 2018; Volume 538.
39. Alkhafaji, A.S.; Al-hayder, A.; Hassooni, A. Hybrid IWOPSO Optimization Based Marine Engine Rotational Speed Control Automatic System. *Int. J. Electr. Comput. Eng.* **2020**, *10*, 840–848. [CrossRef]
40. Chen, H.; Xie, J.; Han, J.; Shi, W.; Charpentier, J.-F.; Benbouzid, M. Position Control of Heave Compensation for Offshore Cranes Based on a Particle Swarm Optimized Model Predictive Trajectory Path Controller. *J. Mar. Sci. Eng.* **2022**, *10*, 1427. [CrossRef]
41. Zhu, M.; Sun, W.; Hahn, A.; Wen, Y.; Xiao, C.; Tao, W. Adaptive Modeling of Maritime Autonomous Surface Ships with Uncertainty Using a Weighted LS-SVR Robust to Outliers. *Ocean Eng.* **2020**, *200*, 107053. [CrossRef]

42. Chen, C.; Delefortrie, G.; Lataire, E. Effects of Water Depth and Speed on Ship Motion Control from Medium Deep to Very Shallow Water. *Ocean Eng.* **2021**, *231*, 109102. [CrossRef]
43. Zhu, M.; Tian, K.; Wen, Y.-Q.; Cao, J.-N.; Huang, L. Improved PER-DDPG Based Nonparametric Modeling of Ship Dynamics with Uncertainty. *Ocean Eng.* **2023**, *286*, 115513. [CrossRef]
44. Kijima, K.; Katsuno, T.; Nakiri, Y.; Furukawa, Y. On the Manoeuvring Performance of a Ship with Theparameter of Loading Condition. *J. Soc. Nav. Archit. Jpn.* **1990**, *1990*, 141–148. [CrossRef] [PubMed]
45. Jia, X.; Yang, Y. *Ship Motion Mathematical Model: Modeling Mechanism Modeling and Identification*; Dalian Maritime University Press: Dalian, China, 1999.
46. Broglia, R.; Dubbioso, G.; Durante, D.; Mascio, A.D. Simulation of Turning Circle by CFD: Analysis of Different Propeller Models and Their Effect on Manoeuvring Prediction. *Appl. Ocean Res.* **2013**, *39*, 1–10. [CrossRef]
47. Sun, M.; Zhang, W.; Zhang, Y.; Luan, T.; Yuan, X.; Li, X. An Anti-Rolling Control Method of Rudder Fin System Based on ADRC Decoupling and DDPG Parameter Adjustment. *Ocean Eng.* **2023**, *278*, 114306. [CrossRef]
48. Christofides, P.D.; Scattolini, R.; Muñoz de la Peña, D.; Liu, J. Distributed Model Predictive Control: A Tutorial Review and Future Research Directions. *Comput. Chem. Eng.* **2013**, *51*, 21–41. [CrossRef]
49. Andersen, I.M.V. Wind Loads on Post-Panamax Container Ship. *Ocean Eng.* **2013**, *58*, 115–134. [CrossRef]
50. Zhang, X.; Feng, Y. Control Algorithm of YUPENG Ship Autopilot Based on Tangent Function Nonlinear Feedback. *J. Meas. Sci. Instrum.* **2017**, *8*, 73–78. [CrossRef]
51. Zhang, X. *Simple Robust Control of Ship Motion*; Science Press: Beijing, China, 2012.
52. Kennedy, J.; Eberhart, R. Particle Swarm Optimization. In Proceedings of the ICNN′95—International Conference on Neural Networks, Perth, WA, Australia, 27 November–1 December 1995; Volume 4, pp. 1942–1948.
53. Yasukawa, H.; Yoshimura, Y. Introduction of MMG Standard Method for Ship Maneuvering Predictions. *J. Mar. Sci. Technol.* **2015**, *20*, 37–52. [CrossRef]
54. Zhang, X.; Yang, G.-P.; Zhang, Q. A Kind of Bipolar Sigmoid Function Decorated Nonlinear Ship Course Keeping Algorithm. *J. Dalian Marit. Univ.* **2016**, *42*, 15–19. [CrossRef]